

Study of rare top quark decays into a jet plus a charged pseudo-scalar meson

Long-Shun Lu^{a,b}, Lei-Yi Li^{a,b,c*}, Cai-Dian Lü^{a,b}

^a *Institute of High Energy Physics, CAS, P.O. Box 918(4) Beijing 100049, China*

^b *School of Physics, University of Chinese Academy of Sciences, Beijing 100049, China*

^c *INPAC, Key Laboratory for Particle Astrophysics and Cosmology (MOE),
Shanghai Key Laboratory for Particle Physics and Cosmology,
School of Physics and Astronomy, Shanghai Jiao Tong University, Shanghai 200240, China*

Abstract

The semi-inclusive decay processes of a top quark into a charged pseudo-scalar meson and a jet are studied within the framework of QCD factorization. The leading power of the decay matrix elements can be factorized into heavy-to-light quark transition current and a hadron matrix element up to next-to-leading order QCD corrections. We calculate one-loop virtual corrections together with real gluon emission corrections at the α_s order. The numerical results of the branching ratios are presented for the sum of two-body and three-body decays. We also study the energy cutoff dependence of the gluon jet. These processes are hopeful to be detected in the near future experiments, which can serve as probes for new physics.

*Corresponding author: lileiyi@sjtu.edu.cn

1 Introduction

As the most massive particle in the Standard Model, top quark is believed to be most sensitive to new physics beyond the standard model. The study of top quark decay is one of the most hot topics in both theoretical and experimental studies. Due to its very short lifetime, the top quark decays before hadronization, making it unique among all quarks. Many studies have focused on calculating the dominant decay process $t \rightarrow bW^+$ [1–5], which allows for the determination of intrinsic properties such as the top quark’s mass and lifetime. Recently, there has been growing interest in rare top quark decays [6–14], as these processes are sensitive to new physics and can serve as probes to study beyond the Standard Model [12–14]. Among these decays, a particularly interesting type of rare decays is the top quark semi-inclusive decay [8–11], where the top quark decays into a single high-energy meson and a jet. Theoretically, these processes can be computed perturbatively, while experimentally, different decay channels can be identified by the distinct final states of the meson and jet, enabling their measurement.

There are two distinct types of the semi-inclusive decay channels of the top quark: one involves a final state containing an down-type quark jet and a charged meson $t \rightarrow qM^+$ [8, 9], while the other involves a final state containing a up-type quark jet and a neutral meson $t \rightarrow qM^0$ [9–11]. In Ref. [8, 9], the leading order (LO) results for the top quark semi-inclusive decay processes $t \rightarrow bM^+$ are presented. Ref. [10] calculates the branching ratio for the CKM-suppressed process $t \rightarrow c\Upsilon$ using Non-relativistic QCD (NRQCD), and discusses it in the context of the Minimal Supersymmetric Standard Model. Ref. [11] employs the NRQCD method to calculate the decay of a top quark into a neutral meson and an up-type quark jet, with predictions for potential observation processes $t \rightarrow \bar{B}^0 + \text{jet}$ and $t \rightarrow \bar{B}_s + \text{jet}$ in future experiments.

In this work, we study the top quark semi-inclusive decay $t \rightarrow qP^+$, where $q = d, s, b$ and P^+ denotes a pseudo-scalar meson. The final states of these semi-inclusive decays include mesons, making them suitable for calculation within the framework of QCD factorization [15–21]. The leading order decay amplitude for $t \rightarrow qP^+$ processes can be easily factorized into the decay constant of the final state meson and the heavy-to-light quark current. Given the heavy mass of the top quark, the subleading power ($1/m_t$) corrections to the $t \rightarrow bP^+$ process are small, therefore the next-to-leading-order corrections primarily arise from the QCD loop corrections.

In our study, we calculate the next-to-leading order (NLO) QCD corrections to the $t \rightarrow qP^+$ processes, where the ultraviolet divergences in the loop diagrams are renormalized using dimensional regularization. For the infrared divergences from virtual corrections in these processes, we eliminate them by accounting the real gluon emission. The numerical results indicate that the branching ratios for these processes span the range of $10^{-16} \sim 10^{-7}$. The processes $t \rightarrow b\pi^+$ and $t \rightarrow bD_s^+$ are expected to be measurable at future colliders, such as the

High-Luminosity Large Hadron Collider (HL-LHC) [22], Super Proton-Proton Collider (SPPC) [23, 24] and Future Circular Hadron Collider (FCC-hh) [25]. Some of the CKM-suppressed rare processes are computed for the first time, which could serve as probes for new physics.

The structure of the paper is as follows: the theoretical framework, including the calculation of the one-loop diagrams, is provided in the next section. In the third section, we present the numerical results and a phenomenological discussion, followed by the conclusions in the final section.

2 Theoretical framework

Both the mass of the final-state pseudo-scalar meson m_P and the mass of the final-state jet m_q are much smaller than the mass of the top quark m_t . Therefore, we can safely neglect the final state masses and assume that they lie on the light-cone. The light-cone vectors are defined as

$$n = (1, 0, 0, 1), \quad \bar{n} = (1, 0, 0, -1), \quad (1)$$

which satisfy the relations $n^2 = \bar{n}^2 = 0$ and $n \cdot \bar{n} = 2$. In the light-cone coordinate system, the momentum of the final-state meson is denoted as p , aligned along the light-cone direction, while the momentum of the quark jet is denoted as k , aligned along the anti-collinear direction:

$$p^\mu = \bar{n} \cdot p \frac{n^\mu}{2} + n \cdot p \frac{\bar{n}^\mu}{2} + p_\perp^\mu, \quad k^\mu = \bar{n} \cdot k \frac{n^\mu}{2} + n \cdot k \frac{\bar{n}^\mu}{2} + k_\perp^\mu. \quad (2)$$

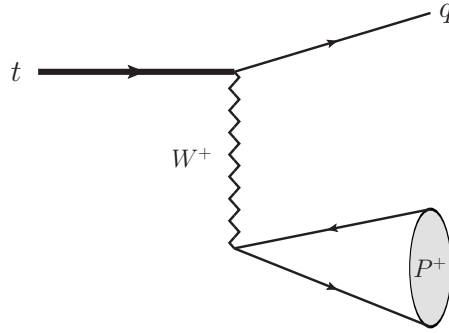


Figure 1: Leading order Feynman diagram for the $t \rightarrow qP^+$ semi-inclusive decay.

In the leading power approximation, $\bar{n} \cdot p = n \cdot k = m_t$ represents the large momentum component, while the other components are power suppressed. The momentum of the top quark is defined as:

$$p_t^\mu = m_t v^\mu, \quad (3)$$

where $v^\mu = (1, 0, 0, 0)$ represents the velocity of the top quark at its rest frame. The tree-level diagram for the semi-inclusive decay process $t \rightarrow qP^+$ is shown in Fig. 1 and the decay

amplitude is

$$\mathcal{A}^{(0)} = -\frac{4G_F}{\sqrt{2}} V_{q_1 q_2} V_{tq}^* \langle P^+(p) | \bar{q}_1 \gamma^\mu P_L q_2 | 0 \rangle \langle q(k) | \bar{q} \gamma_\mu P_L t | t(p_t) \rangle, \quad (4)$$

where V_{tq}^* and $V_{q_1 q_2}$ represent the CKM matrix elements, with the up-type quark $q_1 = u, c$ and the down-type quark $q, q_2 = d, s, b$. The q -jet is generated from the heavy-to-light current of the top quark, while the final-state pseudo-scalar meson is produced from the W -boson. The definition of the decay constant for the pseudo-scalar meson is given by:

$$\langle P^+(p) | \bar{q}_1 \gamma_\mu \gamma_5 q_2 | 0 \rangle = -i f_P p_\mu, \quad (5)$$

where f_P represents the decay constant of the pseudo-scalar meson. In the QCD factorization framework, the tree-level decay amplitudes of $t \rightarrow qP^+$ processes are proportional to the meson decay constant times the quark weak transition current. We then obtain the tree-level decay width of top quark[†]:

$$\Gamma^{(0)} = \frac{G_F^2 m_t^3 f_P^2}{16\pi} |V_{q_1 q_2} V_{tq}^*|^2. \quad (6)$$

2.1 Virtual corrections

As probes for studying new physics, the experimental precision of top quark decay processes in future colliders [22–25] requires necessitating precise calculations of the processes to improve theoretical accuracy. As discussed in the introduction, the power correction is suppressed by $1/m_t$, leading to small corrections, since the mass of the top quark is much larger than the masses of the final-state jet and meson. The QCD loop contributions constitute the main contribution to the next-to-leading-order corrections.

The Feynman diagrams for the NLO QCD corrections to the processes $t \rightarrow qP^+$ are shown in Fig. 2. In diagrams (b) to (e), the colored gluon is coupled to the final-state meson which is a color singlet state; thus, the contributions from these diagrams are zero. Diagram (f) can be absorbed into the definition of decay constants in Eq. (5). Therefore, for the process $t \rightarrow qP^+$, it suffices to consider only diagram (a), and the one-loop result for the decay amplitude still retains the factorization formalism as the tree-level in Eq. (4). To address the ultraviolet divergences at the amplitude level, we employ dimensional regularization for subtraction, working in $D = 4 - 2\epsilon$ dimension. Under the conditions of on-shell renormalization, the wave function of the top quark is renormalized as follows:

$$Z_t = 1 - \frac{\alpha_s(\mu)}{4\pi} C_F \left(\frac{4\pi\mu^2}{m_t^2} \right)^\epsilon \left(\frac{3}{\epsilon} + 4 - 3\gamma \right). \quad (7)$$

[†]Our formula differs by a factor of $1/9$ from that in Ref. [8], while agreeing with the updated version of Ref. [9].

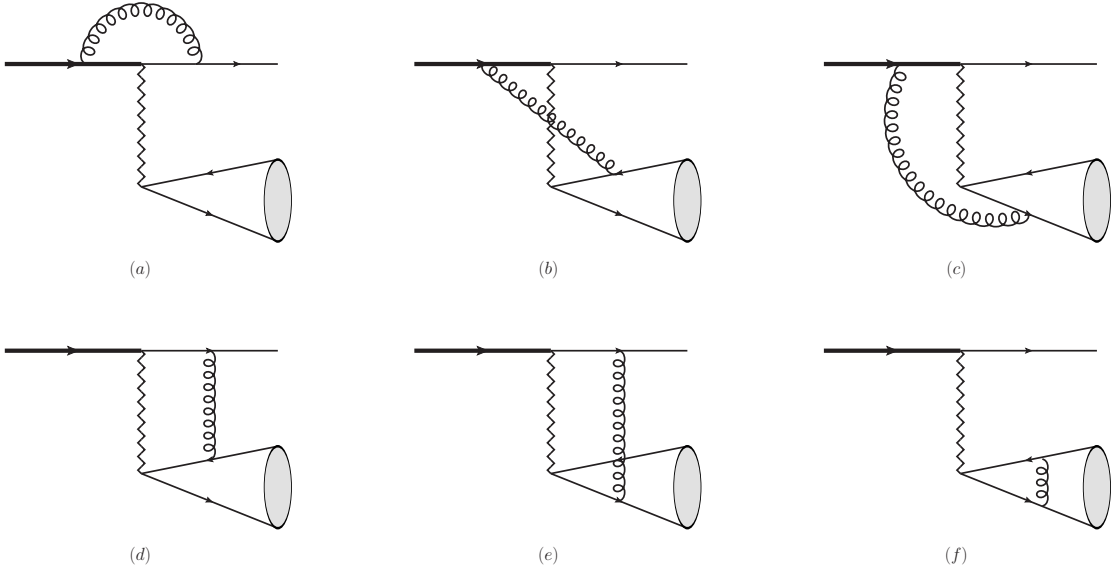


Figure 2: Virtual correction for semi-inclusive processes of $t \rightarrow qP^+$

where γ is the Euler's constant. For the quark jet, we neglect its mass, resulting in renormalization constant $Z_q = 1$. Taking the renormalization into account, the ultraviolet divergences in our loop diagram calculation can be removed in the standard way.

For the infrared divergence, we also work in the dimensional regularization. The decay width in D -dimension for the NLO QCD correction can be expressed as:

$$\Gamma_{\text{virtual}}^{(1)} = -\frac{\Gamma^{(0)}}{m_t^{2\epsilon}} \left[\frac{\alpha_s(\mu)}{3\pi} \left(\frac{4\pi\mu}{m_t} \right)^{2\epsilon} \left(\frac{2}{\epsilon^2} + \frac{9-4\gamma}{\epsilon} + 4\gamma^2 - 18\gamma - \frac{\pi^2}{3} + 30 \right) \right], \quad (8)$$

where $1/m_t^{2\epsilon}$ is from the two-body phase space integral in dimensions D [26]. The remaining divergent terms in Eq. (8) correspond to infrared divergences, which require additional subtraction from real gluon emission contributions.

2.2 Real gluon correction

As a semi-inclusive process, $t \rightarrow qP^+$ involves a heavy-to-light current $t \rightarrow q$ that exhibits a single-jet effect. The radiation of real gluons contributes to the decay width at order $\mathcal{O}(\alpha_s)$, the same order as the virtual correction, to be considered together. In the calculations of Section 2.1, we neglected the mass of the bottom quark. Under the leading order of $1/m_t$ power expansion, this introduces soft and collinear divergences, necessitating the introduction of real corrections for subtraction. The Feynman diagrams for real gluon radiation in the $t \rightarrow qP^+$ process are shown in Fig. 3. The decay width of the three body decay resulting from

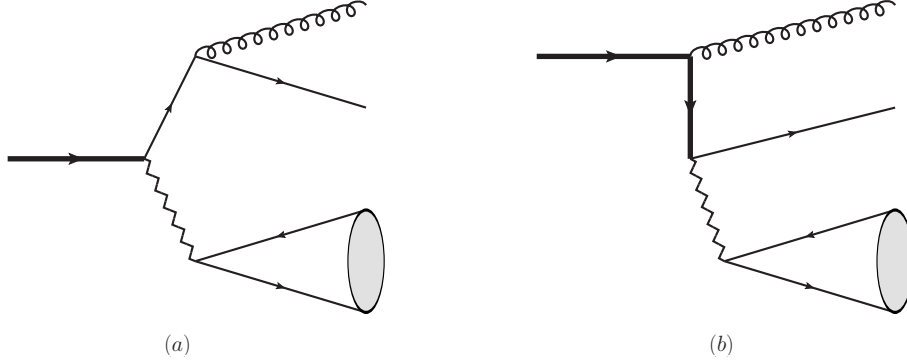


Figure 3: Real gluon emission for the semi-inclusive processes of $t \rightarrow qP^+$

the real gluon radiation in D -dimensions is given by:

$$\Gamma_{\text{real}}^{(1)} = \frac{\Gamma^{(0)}}{m_t^{2\epsilon}} \left[\frac{\alpha_s(\mu)}{3\pi} \left(\frac{4\pi\mu}{m_t} \right)^{2\epsilon} \left(\frac{2}{\epsilon^2} - \frac{4\gamma - 9}{\epsilon} - 18\gamma + 4\gamma^2 - \frac{5}{3}\pi^2 + 35 \right) \right], \quad (9)$$

where $1/m_t^{2\epsilon}$ is from the three-body phase space integral in dimension D [26]. It is easy to see that the infrared divergences in the decay amplitude with virtual corrections in Eq. (8) can be canceled by the real gluon corrections from three-body radiation in Eq. (9), if we sum the one-loop corrections for the two-body decay and three-body decay processes. In this way, we obtain a finite total decay width at the α_s order:

$$\Gamma = \Gamma^{(0)} + \Gamma_{\text{virtual}}^{(1)} + \Gamma_{\text{real}}^{(1)} = \Gamma^{(0)} \left[1 + \frac{\alpha_s(\mu)}{3\pi} \left(-\frac{4}{3}\pi^2 + 5 \right) \right] + \mathcal{O}(\alpha_s^2), \quad (10)$$

which is in agreement with the result presented in Ref. [1].

2.3 Gluon energy cutoff

In the calculations of the previous section, we included the contributions from three-body radiation corrections to cancel the infrared divergences, which introduces part of the three-body corrections. In hadron colliders, there are too many jets from QCD background. Experimentally the signal background ratio for two jets final state is lower than the single jet final state. In any detector, there is an energy cut for a jet. Thus in our case, if the gluon jet energy is below the detector's gluon energy threshold, experiments treat this event as two body decay, even if theoretically it is three body decay. To compare with experimental results, it is necessary to subtract the contributions from real gluons with energies above the detector's gluon energy threshold.

In the semi-inclusive decay of the top quark, other heavy-to-light currents are suppressed by the CKM matrix element compared to $t \rightarrow b$ current, and collider experiments have better

resolution for b -jets than that for light-quark jets. This makes the corresponding processes the most likely to be experimentally observed. Therefore, we further consider an energy cutoff [34] in the $t \rightarrow b\pi^+$ and $t \rightarrow bD_s^+$ processes to subtract the three-body effects above the detector threshold, allowing for a direct comparison with collider experiment results. While the energy cutoff can eliminate soft divergences, collinear divergences still exist. To address this issue, we can simply retain the pole mass of the bottom quark as a collinear regulator to avoid collinear divergences,

$$\Gamma_{\text{real}}^{(1),\text{cut}} = \frac{1}{2m_t} \int d\Pi \frac{1}{3} \sum_{\text{color}} \frac{1}{2} \sum_{\text{spin}} \sum_{\epsilon} |\mathcal{A}_{\text{real}}|^2, \quad (11)$$

where ϵ is the polarization of gluon. The decay amplitude $\mathcal{A}_{\text{real}}$ can simply read from Fig. 3. For discrete the three body decay from the dominant two body decay as in [34], we take a gluon energy cut δ in the three body phase space integral to get the numerical result of three body decay. We chose dimensionless variables of b -jet as x_b , gluon jet as x_g , pseudo-scalar meson as x_P [26]

$$x_b = \frac{2k \cdot p_t}{m_t^2} = \frac{2E_b}{m_t}, \quad x_P = \frac{2p \cdot p_t}{m_t^2} = \frac{2E_P}{m_t}, \quad x_g = \frac{2l \cdot p_t}{m_t^2} = \frac{2E_g}{m_t}, \quad (12)$$

where l is the momentum of gluon jet, E_b , E_g and E_P are the energy of the b -jet, gluon jet and pseudo-scalar meson respectively. Since we chose δ as the cut of gluon jet, so the minimum of the gluon energy is $E_{g,\min} = \delta$, and the range of these variables are

$$\begin{aligned} x_g : \frac{2\delta}{m_t} &\sim \frac{m_t^2 - m_b^2}{m_t^2}, \\ x_b : \frac{2m_b}{m_t} &\sim \frac{m_t^2 + m_b^2}{m_t^2}, \\ x_P : 0 &\sim \frac{m_t^2 - 2\delta m_t - m_b^2}{m_t(m_t - 2\delta)}. \end{aligned} \quad (13)$$

After transforming the three-body phase space integral in Eq. (11) into an integral over momentum fractions, we can compute the decay width of real gluon radiation above the threshold $\Gamma_{\text{real}}^{(1),\text{cut}}$. Taking into account the results from Eq. (10) and (11), we finally obtain the decay width with the energy cutoff:

$$\Gamma_{t \rightarrow bP^+} = \Gamma - \Gamma_{\text{real}}^{(1),\text{cut}} + \mathcal{O}(\alpha_s^2). \quad (14)$$

3 Numerical results

In the calculation of the previous section, we presented the decay width for $t \rightarrow qP^+$ up to $\mathcal{O}(\alpha_s)$. To compute the numerical results for the branching ratios, we need to introduce

Table 1: Input parameters in the numerical calculations.

$f_\pi = 130.2 \pm 0.8 \text{ MeV}$	[27]	$f_K = 155.7 \pm 0.7 \text{ MeV}$	[27]
$f_D = 212.0 \pm 0.7 \text{ MeV}$	[27]	$f_{D_s} = 249.9 \pm 0.5 \text{ MeV}$	[27]
$f_B = 190.0 \pm 1.30 \text{ MeV}$	[27]	$f_{B_c} = 434.0 \pm 15.0 \text{ MeV}$	[28]
$G_F = 1.1663788 \times 10^{-5} \text{ GeV}^{-2}$	[29]	$\Gamma_t = 1.42^{+0.19}_{-0.15} \text{ GeV}$	[29]
$m_t = 172.57 \pm 0.29 \text{ GeV}$	[29]	$m_b = 4.78 \pm 0.06 \text{ GeV}$	[29]
$ V_{ud} = 0.97367 \pm 0.00032$	[29]	$ V_{us} = 0.22431 \pm 0.00085$	[29]
$ V_{ub} = (3.82 \pm 0.20) \times 10^{-3}$	[29]	$ V_{cd} = 0.221 \pm 0.004$	[29]
$ V_{cs} = 0.975 \pm 0.006$	[29]	$ V_{cb} = (41.1 \pm 1.2) \times 10^{-3}$	[29]
$ V_{td} = (8.6 \pm 0.2) \times 10^{-3}$	[29]	$ V_{ts} = (41.5 \pm 0.9) \times 10^{-3}$	[29]
$ V_{tb} = 1.010 \pm 0.027$	[29]		

input parameters, which are detailed in Table 1. The strong coupling constant is chosen as $\alpha_s(\hat{m}_t) = 0.1090 \pm 0.0014$ [29]. According to the Eq. (6) and (10), the numerical results for the decay width at LO and NLO precision are shown in Table 2. The NLO corrections contribute approximately 10% compared to LO one. Some of the decay channels have been calculated at LO in Ref. [8, 9]. We list their results[‡] also in Table 2. There exists nearly an order-of-magnitude discrepancy between the results in [8] and ours, originating from a difference by a factor of 1/9 in Eq. (6).

Among all the decay channels, $t \rightarrow b\pi^+$ and $t \rightarrow bD_s^+$ processes have the largest branching ratios. Recent experiments have indicated that the decay processes of the D_s meson series can be measured at the LHC using the ATLAS [30] and CMS [31] detectors. At the high luminosity LHC in the near future, the experiments with the highest top quark production rates are the ATLAS and CMS collaborations. The processes $t \rightarrow b\pi^+$ and $t \rightarrow bD_s^+$ are the most likely to be measured in near future experiments. Other decay processes are possible to be detected in future collider SPPC [23, 24] and FCC-hh [25] with very high energy and high luminosity [9].

[‡]The authors of Ref. [9] have corrected the 1/9 factor discrepancy recently and updated their data, establishing consistency with our results.

Table 2: Branching fractions of top quark semi-inclusive decay at leading order (LO) and next-to-leading order precision (NLO), comparing with previous results.

Branching fraction	LO (This work)	NLO (This work)	LO [8]	LO [9]
$\text{Br}(t \rightarrow b\pi^+)$	$1.60^{+0.19}_{-0.23} \times 10^{-7}$	$1.45^{+0.17}_{-0.21} \times 10^{-7}$	4.0×10^{-8}	1.6×10^{-7}
$\text{Br}(t \rightarrow bK^+)$	$1.22^{+0.14}_{-0.18} \times 10^{-8}$	$1.10^{+0.13}_{-0.16} \times 10^{-8}$	—	1.2×10^{-8}
$\text{Br}(t \rightarrow bD^+)$	$2.20^{+0.27}_{-0.33} \times 10^{-8}$	$1.99^{+0.25}_{-0.30} \times 10^{-8}$	—	2.3×10^{-8}
$\text{Br}(t \rightarrow bD_s^+)$	$5.93^{+0.71}_{-0.86} \times 10^{-7}$	$5.37^{+0.64}_{-0.78} \times 10^{-7}$	2.0×10^{-7}	6.0×10^{-7}
$\text{Br}(t \rightarrow bB^+)$	$5.26^{+0.84}_{-0.94} \times 10^{-12}$	$4.77^{+0.76}_{-0.85} \times 10^{-12}$	—	5.3×10^{-12}
$\text{Br}(t \rightarrow bB_c^+)$	$3.18^{+0.47}_{-0.54} \times 10^{-9}$	$2.88^{+0.43}_{-0.49} \times 10^{-9}$	—	3.1×10^{-9}
$\text{Br}(t \rightarrow s\pi^+)$	$2.71^{+0.31}_{-0.38} \times 10^{-10}$	$2.46^{+0.28}_{-0.35} \times 10^{-10}$	—	—
$\text{Br}(t \rightarrow sK^+)$	$2.06^{+0.24}_{-0.29} \times 10^{-11}$	$1.86^{+0.21}_{-0.26} \times 10^{-11}$	—	—
$\text{Br}(t \rightarrow sD^+)$	$3.70^{+0.44}_{-0.54} \times 10^{-11}$	$3.35^{+0.40}_{-0.49} \times 10^{-11}$	—	—
$\text{Br}(t \rightarrow sD_s^+)$	$1.00^{+0.12}_{-0.14} \times 10^{-9}$	$9.07^{+1.04}_{-1.28} \times 10^{-10}$	—	—
$\text{Br}(t \rightarrow sB^+)$	$8.89^{+1.38}_{-1.56} \times 10^{-15}$	$8.05^{+1.25}_{-1.42} \times 10^{-15}$	—	—
$\text{Br}(t \rightarrow sB_c^+)$	$5.37^{+0.78}_{-0.90} \times 10^{-12}$	$4.86^{+0.71}_{-0.81} \times 10^{-12}$	—	—
$\text{Br}(t \rightarrow d\pi^+)$	$1.16^{+0.14}_{-0.17} \times 10^{-11}$	$1.05^{+0.12}_{-0.15} \times 10^{-11}$	—	—
$\text{Br}(t \rightarrow dK^+)$	$8.84^{+1.03}_{-1.26} \times 10^{-13}$	$8.00^{+0.93}_{-1.14} \times 10^{-13}$	—	—
$\text{Br}(t \rightarrow dD^+)$	$1.59^{+0.19}_{-0.23} \times 10^{-12}$	$1.44^{+0.17}_{-0.21} \times 10^{-12}$	—	—
$\text{Br}(t \rightarrow dD_s^+)$	$4.30^{+0.50}_{-0.61} \times 10^{-11}$	$3.90^{+0.45}_{-0.55} \times 10^{-11}$	—	—
$\text{Br}(t \rightarrow dB^+)$	$3.82^{+0.60}_{-0.67} \times 10^{-16}$	$3.46^{+0.54}_{-0.61} \times 10^{-16}$	—	—
$\text{Br}(t \rightarrow dB_c^+)$	$2.31^{+0.34}_{-0.39} \times 10^{-13}$	$2.09^{+0.31}_{-0.35} \times 10^{-13}$	—	—

The energy threshold for jets are usually detector dependent [32, 33]. In our calculation, we set the gluon energy cutoff thresholds to $\delta=20, 25, 30$ GeV, respectively. The branching

Table 3: Branching fractions of $t \rightarrow b\pi^+$ and $t \rightarrow bD_s^+$ decay with gluon energy cut $\delta = 20, 25, 30$ GeV, respectively.

Branching fraction	NLO ($\delta = 20\text{GeV}$)	NLO ($\delta = 25\text{GeV}$)	NLO ($\delta = 30\text{GeV}$)
$\text{Br}(t \rightarrow b\pi^+)$	$8.39_{-1.09}^{+1.10} \times 10^{-8}$	$9.89 \pm 1.29 \times 10^{-8}$	$1.10 \pm 0.14 \times 10^{-7}$
$\text{Br}(t \rightarrow bD_s^+)$	$3.10_{-0.40}^{+0.41} \times 10^{-7}$	$3.65 \pm 0.48 \times 10^{-7}$	$4.05 \pm 0.53 \times 10^{-7}$

ratios of $t \rightarrow b\pi^+$ and $t \rightarrow bD_s^+$ processes with such different energy cuts of $\Gamma_{t \rightarrow bP^+}$ in Eq. (14) are presented in Table 3. To avoid collinear divergences in our calculation, we retain the mass of the bottom quark [34] in the $t \rightarrow b\pi^+$ and $t \rightarrow bD_s^+$ processes. From Table 3, one can see that the branching ratios of experimental detectable two body decays have around 20% differences for different energy cut of gluon jet.

For the future collider HL-LHC, running at a center-of-mass energy of $\sqrt{s} = 14$ TeV, the total integrated luminosity is expected to be 3 ab^{-1} [22], with the top quark pair production cross section approximately $\sigma_{t\bar{t}}^{\text{HL-LHC}} = 1 \text{ nb}$ [25]. For the future collider FCC-hh, the integrated luminosity is projected to be 20 ab^{-1} [25] at energies $\sqrt{s} = 100$ TeV, with the top quark pair production cross section around $\sigma_{t\bar{t}}^{\text{FCC-hh}} = 35 \text{ nb}$ [25]. Based on the total production cross section and integrated luminosity for future colliders, the number of generated events can be estimated using the formula provided in Ref. [11] :

$$N_{\text{event}} = \sigma_{t\bar{t}} \times \mathcal{L}_{\text{int}} \times \text{Br}(t \rightarrow qP^+), \quad (15)$$

where \mathcal{L}_{int} is the total the integrated luminosity of future collider. Based on the branching fraction with the cutoff in Table 3, it can be seen that the number of events for the $t \rightarrow b\pi^+$ and $t \rightarrow bD_s^+$ processes at the HL-LHC is expected to be in the range of $10^2 \sim 10^3$, making their detection possible in the near future. For the future collider FCC-hh, the event yield for these two dominant rare decay channels is projected to be in the range of $10^4 \sim 10^5$, providing a sufficient dataset for precise tests of these processes. These two rare decay processes can be used to test the QCD factorization theorem in top quark semi-inclusive decays, as well as serve as probes for new physics.

4 Conclusion

In this work, we have calculated the NLO corrections to the top quark semi-inclusive decay $t \rightarrow qP^+$. Within the framework of QCD factorization, the leading power matrix element is factorized into inclusive and exclusive components up to NLO. The ultraviolet and infrared

Table 4: The estimation of the event numbers for the top quark semi-inclusive decay processes at future colliders.

Event number	NLO ($\delta = 20\text{GeV}$)	NLO ($\delta = 25\text{GeV}$)	NLO ($\delta = 30\text{GeV}$)
$N_{\text{even}}^{\text{HL-LHC}}(t \rightarrow b\pi^+)$	2.5×10^2	3.0×10^2	3.3×10^2
$N_{\text{even}}^{\text{HL-LHC}}(t \rightarrow bD_s^+)$	9.3×10^2	1.1×10^3	1.2×10^3
$N_{\text{even}}^{\text{FCC-hh}}(t \rightarrow b\pi^+)$	5.9×10^4	6.9×10^4	7.7×10^4
$N_{\text{even}}^{\text{FCC-hh}}(t \rightarrow bD_s^+)$	2.2×10^5	2.6×10^5	2.8×10^5

divergences at NLO are canceled in the computation of the leading power decay width. We present numerical results for the branching fractions of the two body semi-inclusive processes, including the corresponding real gluon emission three body decays. The branching ratios for these processes span a wide range, from 10^{-16} to 10^{-7} , due to quite different CKM matrix elements.

For the $t \rightarrow b\pi^+$ and $t \rightarrow bD_s^+$ processes, with the largest CKM matrix elements, we provide their branching ratio dependence on the cutoff gluon energy, anticipating that they could be measured at the near future experiments. These results provide a chance to test the factorization theorem in semi-inclusive processes, which could also serve as a probe for new physics.

Acknowledgment

We are grateful to Dong-Hao Li for helpful discussions. The work is supported in part by the National Key Research and Development Program of China (2023YFA1606000) and by the National Natural Science Foundation of China under Grant No. 12447185, 12275277 and 12435004.

References

- [1] M. Jezabek and J. H. Kuhn, *Nucl. Phys. B* **314**, 1 (1989).
- [2] A. Czarnecki, *Phys. Lett. B* **252**, 467 (1990).
- [3] C. S. Li, R. J. Oakes, and T. C. Yuan, *Phys. Rev. D* **43**, 3759 (1991).
- [4] J. Gao, C. S. Li, and H. X. Zhu, *Phys. Rev. Lett.* **110**, 042001 (2013), [arXiv:1210.2808 \[hep-ph\]](#) .
- [5] L.-B. Chen, H. T. Li, Z. Li, J. Wang, Y. Wang, and Q.-f. Wu, *Phys. Rev. D* **109**, L071503 (2024), [arXiv:2309.00762 \[hep-ph\]](#) .
- [6] L. T. Handoko, *Nuovo Cim. A* **111**, 1275 (1998), [arXiv:hep-ph/9803262](#) .
- [7] L. T. Handoko and J. Hashida, *Phys. Rev. D* **58**, 094008 (1998), [arXiv:hep-ph/9803265](#) .
- [8] M. Beneke *et al.*, in *Workshop on Standard Model Physics (and more) at the LHC (First Plenary Meeting)* (2000) pp. 419–529, [arXiv:hep-ph/0003033](#) .
- [9] d’Enterria, David and Le, Van Dung [10.1088/1361-6471/ad3c59](#) (2023), [arXiv:2312.11211 \[hep-ph\]](#) .
- [10] L. T. Handoko and C.-F. Qiao, *J. Phys. G* **27**, 1391 (2001), [arXiv:hep-ph/9907375](#) .
- [11] D. d’Enterria and H.-S. Shao, *JHEP* **07**, 127, [arXiv:2005.08102 \[hep-ph\]](#) .
- [12] J. J. Liu, C. S. Li, L. L. Yang, and L. G. Jin, *Phys. Lett. B* **599**, 92 (2004), [arXiv:hep-ph/0406155](#) .
- [13] F.-M. Cai, S. Funatsu, X.-Q. Li, and Y.-D. Yang, *Eur. Phys. J. C* **82**, 881 (2022), [arXiv:2202.08091 \[hep-ph\]](#) .
- [14] F.-M. Cai, R.-L. Fan, X.-Q. Li, and Y.-D. Yang, (2024), [arXiv:2409.04179 \[hep-ph\]](#) .
- [15] M. Beneke, G. Buchalla, M. Neubert, and C. T. Sachrajda, *Phys. Rev. Lett.* **83**, 1914 (1999), [arXiv:hep-ph/9905312](#) .
- [16] M. Beneke, G. Buchalla, M. Neubert, and C. T. Sachrajda, *Nucl. Phys. B* **606**, 245 (2001), [arXiv:hep-ph/0104110](#) .
- [17] H.-Y. Cheng and A. Soni, *Phys. Rev. D* **64**, 114013 (2001), [arXiv:hep-ph/0105246](#) .
- [18] M. Beneke and M. Neubert, *Nucl. Phys. B* **675**, 333 (2003), [arXiv:hep-ph/0308039](#) .

- [19] Y. Grossman, M. König, and M. Neubert, *JHEP* **04**, 101, [arXiv:1501.06569 \[hep-ph\]](#) .
- [20] S. Alte, M. König, and M. Neubert, *JHEP* **02**, 162, [arXiv:1512.09135 \[hep-ph\]](#) .
- [21] C.-D. Lü, Y.-L. Shen, C. Wang, and Y.-M. Wang, *Nucl. Phys. B* **990**, 116175 (2023), [arXiv:2202.08073 \[hep-ph\]](#) .
- [22] G. Apollinari, O. Brüning, T. Nakamoto, and L. Rossi, *CERN Yellow Rep.* , 1 (2015), [arXiv:1705.08830 \[physics.acc-ph\]](#) .
- [23] T. C. S. Group, Cepc conceptual design report: Volume 1 - accelerator (2018), [arXiv:1809.00285 \[physics.acc-ph\]](#) .
- [24] J. Tang, Y. Zhang, Q. Xu, J. Gao, X. Lou, and Y. Wang, in *Snowmass 2021* (2022) [arXiv:2203.07987 \[hep-ex\]](#) .
- [25] A. Abada *et al.* (FCC), *Eur. Phys. J. ST* **228**, 755 (2019).
- [26] M. D. Schwartz, *Quantum Field Theory and the Standard Model* (Cambridge University Press, 2014).
- [27] Y. Aoki *et al.* (Flavour Lattice Averaging Group (FLAG)), (2024), [arXiv:2411.04268 \[hep-lat\]](#) .
- [28] B. Colquhoun, C. T. H. Davies, R. J. Dowdall, J. Kettle, J. Koponen, G. P. Lepage, and A. T. Lytle (HPQCD), *Phys. Rev. D* **91**, 114509 (2015), [arXiv:1503.05762 \[hep-lat\]](#) .
- [29] S. Navas *et al.* (Particle Data Group), *Phys. Rev. D* **110**, 030001 (2024).
- [30] G. Aad *et al.* (ATLAS), *Nucl. Phys. B* **907**, 717 (2016), [arXiv:1512.02913 \[hep-ex\]](#) .
- [31] V. Mariani (CMS), *PoS ICHEP2020*, 399 (2021).
- [32] A. M. Sirunyan *et al.* (CMS), *JINST* **15** (10), P10017, [arXiv:2006.10165 \[hep-ex\]](#) .
- [33] G. Aad *et al.* (ATLAS), *JINST* **19** (06), P06029, [arXiv:2401.06630 \[hep-ex\]](#) .
- [34] N. Quintero, J. L. Diaz-Cruz, and G. Lopez Castro, *Phys. Rev. D* **89**, 093014 (2014), [arXiv:1403.3044 \[hep-ph\]](#) .